PHYSICAL REVIEW D **90,** 055007 (2014)

LHC search for di-Higgs decays of stoponium and other scalars in events with two photons and two bottom jets

Nilanjana Kumar[1] and Stephen P. Martin[1,2]

[1]*Department of Physics, Northern Illinois University, DeKalb, Illinois 60115, USA*
[2]*Fermi National Accelerator Laboratory, P.O. Box 500, Batavia, Illinois 60510, USA*

(Received 15 April 2014; published 8 September 2014)

We study the prospects for LHC discovery of a narrow resonance that decays to two Higgs bosons, using the final state of two photons and two bottom jets. Our work is motivated in part by a scenario in which two-body flavor-preserving decays of the top squark are kinematically forbidden. Stoponium, a hadronic bound state of the top squark and its antiparticle, will then form, and may have a large branching fraction into the two Higgs boson final state. We estimate the cross section needed for a 5-sigma discovery at the 14 TeV LHC for such a narrow di-Higgs resonance, using the invariant mass distributions of the final state bottom jets and photons, as a function of the integrated luminosity. The results are also applicable to any other di-Higgs resonance produced by gluon fusion.

DOI: 10.1103/PhysRevD.90.055007 PACS numbers: 12.60.-i

I. INTRODUCTION

ATLAS [1,2] and CMS [3,4] have confirmed the existence of a resonance with properties that are consistent with a minimal standard model Higgs scalar boson, h, with a mass near 126 GeV. The precise value of m_h is already known at roughly the 1% level, and will surely improve in the future. This provides an opportunity to search for new physics that lies beyond the standard model, by looking for new heavy particles that decay into h, exploiting the Higgs boson as a standard candle.

One such possibility is stoponium, $\eta_{\tilde{t}}$, a bound state of a top squark (stop) and its antiparticle. The stop will be stable enough to hadronize provided that it has no flavor-preserving two-body decays. The binding energy of the $J^{PC} = 0^{++}$ ground state of stoponium is of order a few GeV, and its width is typically about 2 orders of magnitude smaller. It will decay primarily by annihilation into pairs of standard model particles, including final states gg, WW, ZZ, hh, $\gamma\gamma$, $Z\gamma$, $t\bar{t}$, and $b\bar{b}$, as well as pairs of neutralinos, depending on the masses and the stop mixing angle and other supersymmetry-breaking parameters [5–7]. Therefore one can search for narrow invariant mass peaks of stoponium at the LHC or at future hadron colliders. The diphoton final state, as originally proposed in [5,6] and studied more recently in [7–9], is a promising one due to its clean experimental signature and the excellent diphoton mass resolution of the LHC detectors. The ZZ and WW final states may also provide a viable discovery signature [10,11]. Early work on stoponium at hadron colliders can be found in [12–15], and discussions of stoponium at linear colliders have been presented in [16–18].

If the stop mass is at least a few GeV larger than m_h, then the decay $\eta_{\tilde{t}} \to hh$ is kinematically allowed and also potentially observable [14], and can easily have a branching ratio of tens of percent. This possibility was explored in early work for the case $2m_h < m_{\eta_{\tilde{t}}} < m_W$ in Ref. [14]. In some more modern models, this decay can even have the dominant branching ratio if $m_{\eta_{\tilde{t}}}$ is not too far above the threshold $2m_h$; see for example the model lines in Fig. 8 of Ref. [7], which illustrate cases with $\mathrm{BR}(\eta_{\tilde{t}} \to hh) > 0.7$. The $\mathrm{BR}(\eta_{\tilde{t}} \to hh)$ tends to decrease slowly as $m_{\eta_{\tilde{t}}}$ moves far above threshold. The combination of the rare but clean decay $h \to \gamma\gamma$ and the high branching ratio decay $h \to b\bar{b}$ may provide the best opportunity to observe this mode. In this paper, we will therefore explore the ability of the LHC to discover stoponium through $pp \to \eta_{\tilde{t}} \to hh \to \gamma\gamma b\bar{b}$. This could either be an alternative discovery mode, or perhaps a confirmation of a discovery of stoponium in the $\eta_{\tilde{t}} \to \gamma\gamma$ or $\eta_{\tilde{t}} \to ZZ$ modes or of open stop pair production.

The stoponium state is produced through gluon fusion, as the near-threshold limit of open stop production. The production cross section was computed through next-to-leading order (NLO) in Ref. [9] in terms of the stoponium wave function at the origin. A resummed next-to-next-to-leading logarithm calculation is provided in [11]; the effects of threshold resummation were found to be small. When needed, we will use the results of [9] for convenience. The remaining uncertainties may well be dominated by the imperfect knowledge of the stoponium wave functions and production of the excited states. We note in particular that Ref. [9] chose to include only the 1s and 2s stoponium states in the production cross section. Although these give most of the production cross section, there could be additional rate contributions coming from production of higher excited states, if those decay to the s-wave states before decaying by annihilation.

More generally, the same signatures used to search for stoponium will apply to any narrow scalar di-Higgs resonance, including the heavier neutral Higgs scalar boson of the minimal supersymmetric standard model (MSSM),

where there is sensitivity especially if $\tan\beta$ is not too large [19–21], as well as other extensions of the standard model Higgs sector [22–24]. The paper [24] contains a study similar to the present one, but with somewhat different motivations and procedures. A recent search by CMS [25] looks for $pp \to H \to hh$, and sets 95% confidence level limits of order 5 pb on the production cross section for H masses below 360 GeV, but using channels other than $bb\gamma\gamma$. In another study by ATLAS [26] it is shown that a good sensitivity can be achieved for $m_H \geq 600$ while looking at resonances decaying via a pair of Higgs bosons to the $b\bar{b}b\bar{b}$ final state, with 19.5 fb^{-1} of proton-proton collision data at $\sqrt{s} = 8$ TeV. In the rest of this paper, we will use η to represent a generic di-Higgs resonance, although stoponium (denoted $\eta_{\tilde{t}}$) is our primary motivation. It should be noted that the signature for di-Higgs production is also used, with different kinematic requirements due to the nonresonant production, in order to study the trilinear Higgs self-coupling as a test of the standard model, for example see [19,20,27–38]. In the present paper this nonresonant standard model di-Higgs production is one of the backgrounds.

There are a variety of model-building motivations for light stops. For example, a light stop is required in the MSSM to enable weak-scale baryogenesis [39]. A light stop scenario is also one way of accommodating the observed dark matter relic density [40,41] through efficient annihilations in the Universe, if the lightest supersymmetric particle (LSP) is bino-like and $m_{\tilde{t}_1} - m_{\tilde{N}_1}$ is much smaller than the top quark mass, as the thermal abundance of dark matter can be reduced in such cases through stop-mediated neutralino annihilations and/or stop coannihilations [42–45]. The mass difference between the lighter stop and the LSP must be small enough to forbid flavor-preserving two-body decays in order to give the observed dark matter abundance. Finally, the naturalness arguments for "more minimal supersymmetry" [46,47] generally incorporate light top squarks as a feature.

Recently, constraints on the light stop scenario have become available from ATLAS [48–50] and CMS [51,52], ruling out significant parts of parameter space, including even cases of stops that are nearly degenerate with the LSP. However, there remain several holes in the exclusions, including the cases $m_{\tilde{t}_1} - m_{\tilde{N}_1} \approx m_W + m_b$ and $m_{\tilde{t}_1} - m_{\tilde{N}_1} \approx m_t$. Projected constraints by theorists reinterpreting other ATLAS and CMS searches claim [53,54] to fill in these holes up to about $m_{\tilde{t}_1} \approx 250$ GeV (so $m_{\eta_{\tilde{t}}} \approx 500$ GeV), even using less than the full data sets of LHC Run 1. However, we prefer to take these exclusion claims as preliminary until and unless they are confirmed by the experimental collaborations. Furthermore, if the stop decays as $\tilde{t}_1 \to jj$ through R-parity violation, where j represents a light quark jet, then there are no exclusions at all [55,56] at present. In this case, it may be that stoponium will be a competitive way to set model-independent limits on light stops for some time. We will consider stoponium masses down to 275 GeV, corresponding to top-squark masses down to about 138 GeV, so that $\eta_{\tilde{t}} \to hh$ is kinematically allowed.

II. EVENT GENERATION AND SIMULATION

We used MADGRAPH 5 [57] to generate events simulating η production and decay, $pp \to \eta \to hh$, in proton-proton collisions at $\sqrt{s} = 14$ TeV. We used the model HEFT, an extension of the tree-level standard model to include an additional scalar, which we interpreted as η, and effective couplings $gg\eta$, ggh, and $\gamma\gamma h$. We modified HEFT to also include a small ηhh coupling to allow the decay of interest, which was then forced at the level of event generation. The production cross section for $pp \to \eta \to hh$ is taken as an input parameter, in order to maximize t he generality of the results. We set the standard model Higgs boson mass to be $m_h = 126$ GeV, and used branching ratios $\mathrm{BR}(h \to b\bar{b}) = 0.57$ and $\mathrm{BR}(h \to \gamma\gamma) = 0.0022$.

In order to improve the statistics, we generated signal events in which one of the h was forced to decay to $b\bar{b}$ and the other to $\gamma\gamma$, and then normalized the resulting event sample according to the branching ratios and the assumed $pp \to \eta \to hh$ production rate just mentioned. We generated 100000 events for each of $m_\eta = 275$, 300, 325, 350, 375, 400, 425, 450, 475, 500, 525, 550, 575, 600, 650, 700, 800, 900, and 1000 GeV in this way. All the signal samples as well as the background samples mentioned below were generated using MADGRAPH 5 and showered with PYTHIA 6 [58].

The possible backgrounds include nonresonant $\gamma\gamma b\bar{b}$ production, as well as $\gamma\gamma c\bar{c}$ and $\gamma\gamma j(b/\bar{b})$ and $\gamma\gamma j(c/\bar{c})$ and $\gamma\gamma jj$ (where $j = g, u, d, s, \bar{u}, \bar{d}, \bar{s}$), and $\gamma\gamma t\bar{t}$ and $\gamma\gamma Z$ and $t\bar{t}h$ and Zh and $b\bar{b}h$ and hh. Production of the hh background includes a triangular and a box diagram, but the effective coupling for the latter is not included in the version of HEFT we used. We therefore normalized the cross section for the hh background to be 40.2 fb, from [24]. In the LHC detectors, electrons are sometimes misidentified as photons. We therefore included backgrounds from the processes $t\bar{t}$ (with two electrons faking photons) and $t\bar{t}\gamma$ (with one electron faking a photon). Here we used a probability of 0.0181 for each electron to fake a photon [59]. We did not include a possible 4-jet background ($jjjj$) because the efficiencies for two jets to faking photons is very low, and the result must also have two light-flavor jets mistagged as b-jets with a rate of order 10^{-6}, and this background tends to be distributed at low photon p_T and invariant masses. We did include backgrounds of the form $j\gamma b\bar{b}$, where one jet fakes a photon. Here, we used probabilities $1/20100$ for a gluon jet and $1/1680$ for a quark jet to fake a photon [60].

In order to obtain good statistics, we found it useful to put a generator-level cut on the minimum and maximum invariant mass of the diphoton pair ($106 < M_{\gamma\gamma} < 146$) in the backgrounds listed above that explicitly include $\gamma\gamma$, because a tighter cut will be imposed at the analysis level anyway. For the $t\bar{t}h$ and Zh and $b\bar{b}h$ backgrounds, we forced h to decay to two photons, and for the hh background we forced one h to decay to $\gamma\gamma$ and the other to decay to $b\bar{b}$, as for the signal. The event samples were normalized accordingly.

For the detector simulation we used DELPHES 3 [61]. We chose a conservative b-tagging efficiency for b-jets of 0.6. The efficiency of mistagging a charm as a b-jet was taken to be 0.1, while for jets initiated by gluons and u, d, s quarks the b-jet mistagging efficiency was chosen to be 0.001.

III. EVENT SELECTION

In the analysis, we first selected events with exactly two b-tagged jets and two photons. The leading and subleading (in transverse momentum, p_T) photon and b-jet are denoted γ_1, γ_2 and b_1, b_2, respectively. We then applied cuts on the p_T, the pseudorapidity η and $\Delta R \equiv \sqrt{(\Delta\eta)^2 + (\Delta\phi)^2}$ as follows, referred to below as event selection **S1**:

(i) $p_T(b_1, b_2) > (40, 30)$ GeV
(ii) $p_T(\gamma_1, \gamma_2) > (35, 25)$ GeV
(iii) $|\eta(b_1, b_2)| < 2.7$
(iv) $|\eta(\gamma_1, \gamma_2)| < 2.5$
(v) $\Delta R_{ij} > 0.5$, for $i, j = b_1, b_2, \gamma_1, \gamma_2$.

The cuts on $b\bar{b}$ invariant mass, p_T and ΔR have been chosen to retain most of the signal while reducing some major sources of background. In particular, we found that reducing the ΔR cuts to 0.4 does not increase the signal acceptance by a significant amount. We performed the whole analysis with various other choices of leading and subleading b-jet p_T's and found that other choices do not provide for a significantly better retention of signal over background.

Given the kinematics of the signal we are interested in, we then applied cuts on the invariant masses of the $\gamma\gamma$ pair, the bb pair, and on the four-body $\gamma\gamma bb$ system. For the last cut, we found that it is better to define a modified invariant mass M_X, according to

$$M_X \equiv M_{bb\gamma\gamma} - M_{bb} + m_h, \tag{3.1}$$

where $m_h = 126$ GeV is the fixed, known Higgs mass. By subtracting off M_{bb} and adding in the true Higgs mass, one tends to mitigate the effects of b-jet momentum mismeasurements. The distribution of M_X has a sharper peak, and is concentrated closer to m_η, than the distribution of $M_{bb\gamma\gamma}$. The sequence of event selection cuts we used is

S2: As in **S1**, with $|M_{\gamma\gamma} - m_h| < 6$ GeV,
S3: As in **S2**, with $|M_{bb} - m_h| < 30$ GeV,
S4: As in **S3**, with $|M_X - m_\eta| < 0.07 m_\eta$, where m_η is the position of the putative peak.

The widths of the $M_{\gamma\gamma}$ and M_{bb} cuts are somewhat larger than the resolutions of a sample of single Higgs boson production, reflecting the performance we observed using DELPHES when the Higgs bosons originate from heavy η decays. Somewhat narrower (wider) windows could perhaps be used for smaller (larger) m_η, although we did not attempt to optimize this, since the optimization is likely to be quite different in real data than in our simulations. The advantage of using M_X rather than the usual four-body invariant mass $M_{bb\gamma\gamma}$ is illustrated in Fig. 1 for signal events that pass the **S3** selection cuts, for $m_\eta = 275$ GeV and for $m_\eta = 500$ GeV. The distributions of M_X as defined in Eq. (3.1), for various different masses m_η are shown in Fig. 2, again after the **S3** selection cuts. It can be seen that the M_X distributions are peaked near the correct η mass, and get wider as m_η increases. For the larger values of m_η, especially above about 700 GeV, the maximum of the M_X distribution occurs somewhat above the true mass, but with a much fatter tail below than above. This is an effect that can be corrected by the experimental collaborations in real data, and in our simulation most events are still within about $\pm 7\%$ of the true value. Here, we expect that in practice a comparison between Monte Carlo simulations and an observed distribution will allow a hypothesis value of m_η to be obtained in cases where a peak is present and

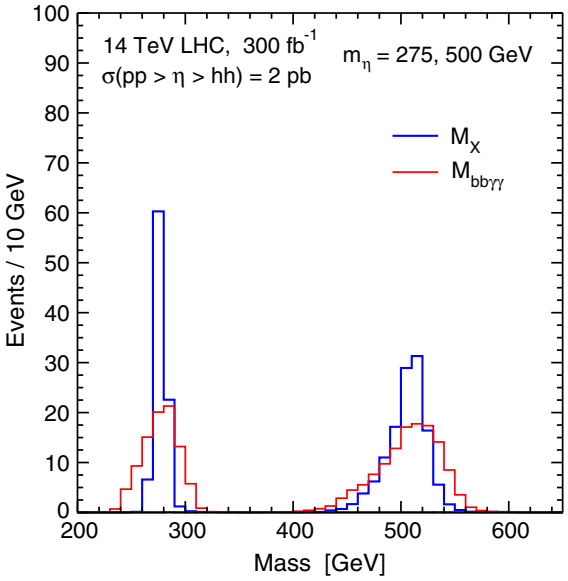

FIG. 1 (color online). Distributions of $M_{bb\gamma\gamma}$ and M_X as defined in Eq. (3.1), for input masses $m_\eta = 275$ GeV and 500 GeV. Both distributions are based on 100 000 signal events $pp \to \eta \to hh$ with one h forced to decay to $\gamma\gamma$ and the other to $b\bar{b}$, and with the distributions normalized by assuming $\sigma \times \mathrm{BR}(pp \to \eta \to hh) = 2$ pb and an integrated luminosity of 300 fb^{-1}. The events were selected with the **S3** cuts.

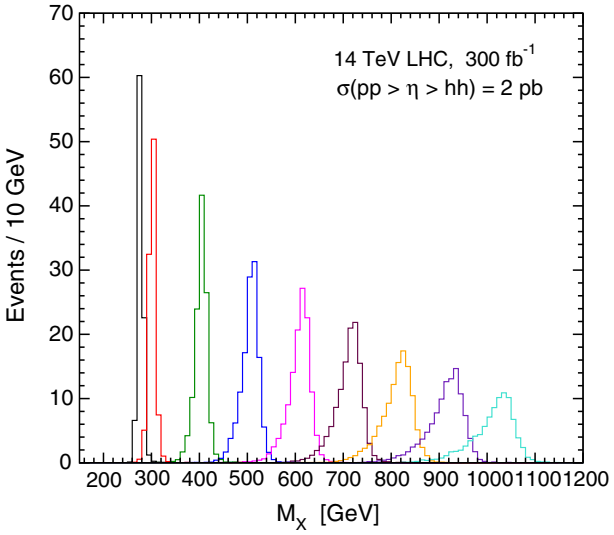

FIG. 2 (color online). Distributions of M_X for $m_\eta = 275$, 300, 400, 500, 600, 700, 800, 900, and 1000 GeV, for signal events, normalized assuming $\sigma \times \mathrm{BR}(pp \to \eta \to hh) = 2$ pb and an integrated luminosity of 300 fb^{-1}, with the event selection **S3** cuts imposed.

large enough to possibly allow a 5-sigma discovery claim. Given the luminosity requirements for a stoponium discovery, one may also expect that evidence for a stop, either in open production or in $\eta_{\tilde{t}} \to \gamma\gamma$ or ZZ will have already accrued to allow for at least a rough estimate of the mass.

The fractions of $pp \to \eta \to hh$ signal events that pass selections **S1**, **S2**, **S3**, and **S4** are given in Table I for various values of m_η. In order to obtain good statistics, the results were obtained for each m_η by generating 100 000 events $pp \to \eta \to hh$ with one h forced to decay to $\gamma\gamma$ and the other forced to decay to $b\bar{b}$, and then normalizing the results using $\mathrm{BR}(h \to \gamma\gamma) = 0.0022$ and $\mathrm{BR}(h \to b\bar{b}) = 0.57$. The nominal fraction of $pp \to \eta \to hh$ that will yield $b\bar{b}\gamma\gamma$ before imposing any selection cuts and efficiencies is $2(0.0022)(0.57) = 0.00253$. After the **S4** selection cuts, the fraction of signal events surviving is of order 2×10^{-4}, and is largest for m_η near 500 GeV.

The backgrounds simulated and the cross sections to pass the selections **S1**, **S2**, **S3**, **S4**, are shown in Table II, for the case that $m_\eta = 275$ GeV. (Only the **S4** selection depends on the choice of m_η.) In Fig. 3, we show for $m_\eta = 275$ GeV the M_{bb} distributions for the signal and the background after applying the selections **S2**, and again after including the **S4** cut on M_X. The latter cut is seen to strongly reduce the background while keeping most of the signal. In Fig. 4 we show the M_X distributions for the total background and for the signal, assuming $\sigma(pp \to \eta \to hh) = 2$ pb, for two choices $m_\eta = 275$ and 500 GeV. The left panel shows the M_X distributions after

TABLE I. The fraction of $pp \to \eta \to hh$ signal events at $\sqrt{s} = 14$ TeV that pass selections **S1**, **S2**, **S3**, and **S4**. The results were obtained for each m_η by generating 100 000 events $pp \to \eta \to hh$ with one h forced to decay to $\gamma\gamma$ and the other forced to decay to $b\bar{b}$, and then normalizing the results using $\mathrm{BR}(h \to \gamma\gamma) = 0.0022$ and $\mathrm{BR}(h \to b\bar{b}) = 0.57$.

$pp \to \eta \to hh$	Fraction $\times 10^4$			
m_η (GeV)	**S1**	**S2**	**S3**	**S4**
275	1.88	1.80	1.52	1.51
300	2.06	1.97	1.63	1.59
325	2.26	2.13	1.72	1.67
350	2.43	2.23	1.79	1.72
375	2.55	2.30	1.84	1.76
400	2.81	2.48	1.96	1.86
425	2.91	2.49	1.98	1.87
450	3.04	2.52	2.01	1.88
475	3.20	2.60	2.08	1.95
500	3.29	2.63	2.11	1.95
525	3.36	2.57	2.08	1.92
550	3.49	2.60	2.10	1.94
575	3.47	2.53	2.05	1.88
600	3.63	2.59	2.12	1.94
650	3.78	2.53	2.07	1.89
700	3.95	2.52	2.09	1.90
800	4.02	2.32	1.95	1.75
900	3.94	2.14	1.82	1.63
1000	3.51	1.84	1.54	1.36

TABLE II. Significant background cross sections after event selections **S1**, **S2**, **S3** and **S4**, for $m_\eta = 275$ GeV. The number of events generated, N_{gen}, is also given. In order to improve statistics, the first seven backgrounds with $\gamma\gamma$ were generated with a cut $|M_{\gamma\gamma} - m_h| < 20$ GeV, while the next four backgrounds were generated with $h \to \gamma\gamma$ forced, and the hh background was generated with one h forced to decay to $\gamma\gamma$ and the other to $b\bar{b}$.

		σ_{pass} (fb)			
Background	N_{gen}	**S1**	**S2**	**S3**	**S4**
$pp \to \gamma\gamma b\bar{b}$	200000	0.944	0.284	0.0861	0.0329
$pp \to \gamma\gamma c\bar{c}$	440000	0.303	0.0912	0.0301	0.0131
$pp \to \gamma\gamma t\bar{t}$	200000	0.119	0.0640	0.0176	0.00449
$pp \to \gamma\gamma j(b/\bar{b})$	200000	0.764	0.233	0.0818	0.0217
$pp \to \gamma\gamma j(c/\bar{c})$	600000	0.369	0.114	0.0337	0.0078
$pp \to \gamma\gamma jj$	1200000	0.540	0.186	0.0723	0.0723
$pp \to \gamma\gamma Z$	200000	0.0462	0.0172	0.00220	0.00052
$pp \to t\bar{t}h$	100000	0.0733	0.0631	0.0171	0.00413
$pp \to Zh$	100000	0.00919	0.00792	0.00329	0.00066
$pp \to b\bar{b}h$	100000	0.0113	0.00992	0.00251	0.00052
$pp \to hh$	100000	0.00927	0.00838	0.00682	0.00212
$pp \to tt$	500000	0.108	0.00748	0.00216	0.00090
$pp \to \gamma tt$	500000	0.157	0.00992	0.00267	0.00086
$pp \to g\gamma b\bar{b}$	500000	0.3522	0.0314	0.0113	0.00411
$pp \to (q/\bar{q})\gamma b\bar{b}$	500000	3.568	0.253	0.0763	0.0173
Total		7.374	1.379	0.446	0.118

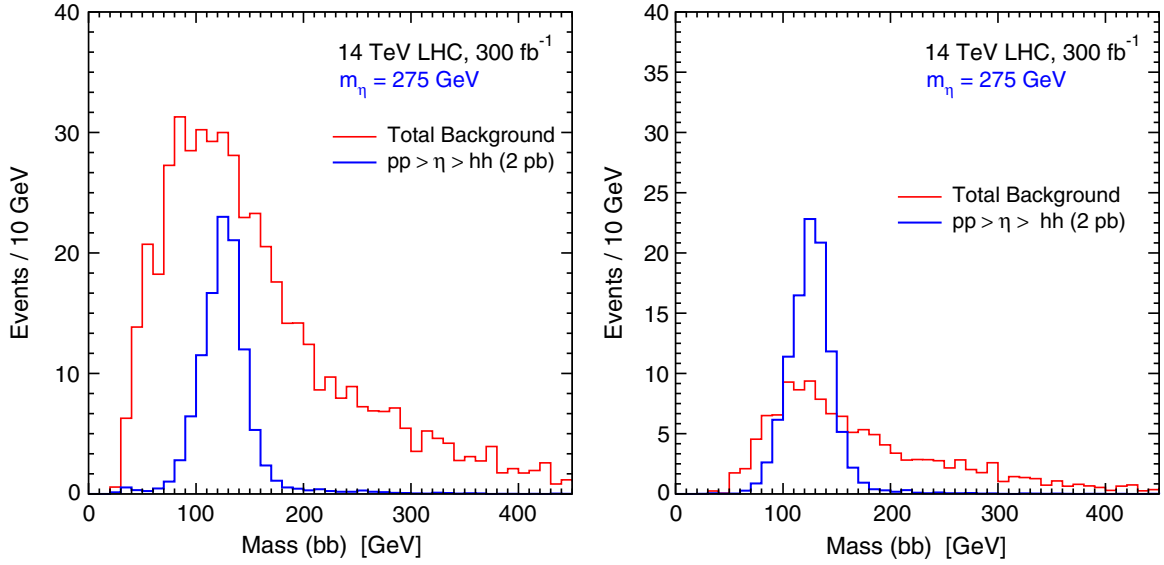

FIG. 3 (color online). The signal and total background distributions of M_{bb}, after applying the **S2** cuts (left panel) and after including in addition the **S4** cut $|M_X - m_\eta| < 0.07 m_\eta$ (right panel), for $m_\eta = 275$ GeV. The normalizations assume 300 fb^{-1} with $\sigma(pp \to \eta \to hh) = 2$ pb.

the event selections **S2**, and the right panel after including the **S3** selection cut on M_{bb}, which clearly helps to give a good discrimination against total background. These distributions are again shown weighted according to 300 fb^{-1} integrated luminosity. Because the event selection **S4** cut depends on the m_η of the putative peak, the background drops significantly with higher masses. This is shown in Table III for $m_\eta = 300$, 400, 500, 600, 700, 800, 900, 1000 GeV. Note that for smaller m_η, the backgrounds are largest for $\gamma\gamma b\bar{b}$ and $\gamma\gamma j(b/\bar{b})$ and $j\gamma b\bar{b}$, but for higher m_η we find that the largest background is $\gamma\gamma jj$ for $j = g, u, d, s, \bar{u}, \bar{d}, \bar{s}$. Clearly these results will be dependent on the ability of the detector analyses to minimize mistags of gluon and light quark jets as b-jets and photons.

The results for the total background cross-sections passing events selection **S4**, as a function of m_η, are plotted in Fig. 5.

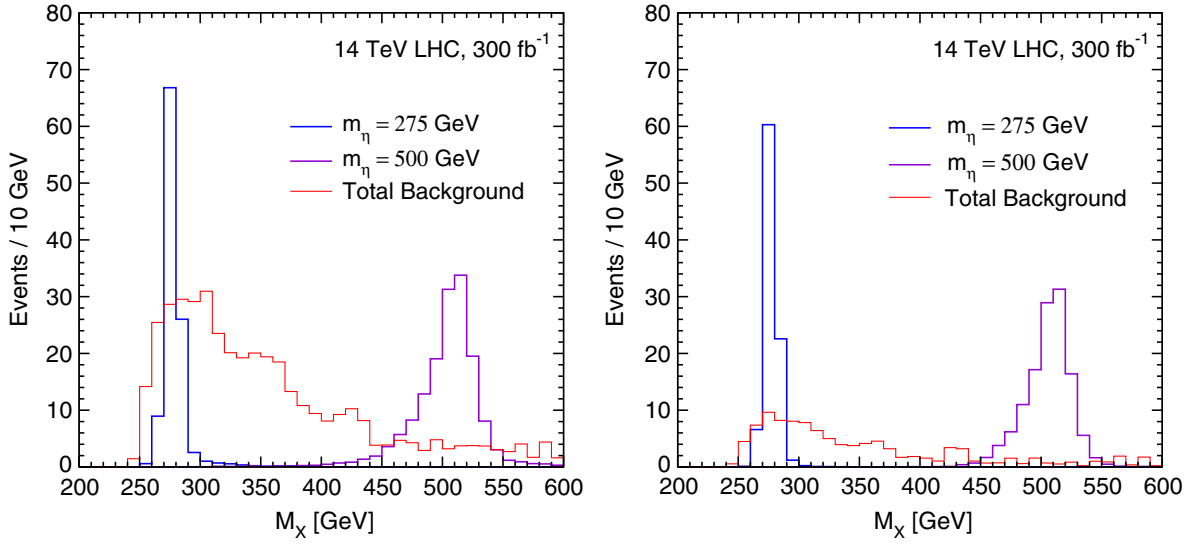

FIG. 4 (color online). The M_X distributions of the total background and the signal are shown after event selections **S2** (left panel) and after **S3** (right panel). For the signal, the distributions are shown for $m_\eta = 275$ GeV and 500 GeV, with $\sigma(pp \to \eta \to hh) = 2$ pb in both cases. The integrated luminosity is taken to be 300 fb^{-1}.

TABLE III. Background cross sections in fb after selections **S4**, for $m_\eta = 300, 400, 500, 600, 700, 800, 900, 1000$ GeV. Cases where no events passed the **S4** selections are listed with $\leq$ and the 1-event cross-section of our sample. For these and other values of m_η, the total backgrounds after the **S4** cuts are shown in Fig. 5 below.

	$\sigma_{\rm pass}$ (fb) for various m_η in GeV							
Background	300	400	500	600	700	800	900	1000
$\gamma\gamma b\bar{b}$	0.0291	0.00797	0.00286	0.00082	0.00061	0.00020	0.00041	0.00010
$\gamma\gamma c\bar{c}$	0.00921	0.00146	0.00048	0.00048	$\leq$0.00048	$\leq$0.00048	$\leq$0.00048	$\leq$0.00048
$\gamma\gamma t\bar{t}$	0.00497	0.00253	0.00104	0.00045	0.00016	0.00010	0.00003	0.00001
$\gamma\gamma j(b/\bar{b})$	0.0199	0.00938	0.00563	0.00338	0.00525	0.00263	0.00075	0.00037
$\gamma\gamma j(c/\bar{c})$	0.01037	0.00648	0.00389	0.00130	$\leq$0.00130	$\leq$0.00130	$\leq$0.00130	$\leq$0.00130
$\gamma\gamma jj$	0.01446	0.00482	0.00482	0.0121	$\leq$0.00241	0.00241	0.00241	0.00482
$\gamma\gamma Z$	0.00036	0.00040	0.00016	0.00012	0.00008	0.00012	$\leq$0.00004	$\leq$0.00004
$t\bar{t}h$	0.00483	0.00255	0.00088	0.00045	0.00024	0.00006	0.00005	0.00002
Zh	0.00066	0.00055	0.00033	0.00018	0.00011	0.00006	0.00002	0.00001
$b\bar{b}h$	0.00050	0.00037	0.00023	0.00013	0.00010	0.00007	0.00003	0.00004
hh	0.00208	0.00080	0.00032	0.00015	0.00005	0.00003	0.00002	0.000004
tt	0.00091	0.00011	0.00002	$\leq 3\times10^{-6}$	$\leq 3\times10^{-6}$	$\leq 3\times10^{-6}$	$\leq 3\times10^{-6}$	$\leq 3\times10^{-6}$
γtt	0.00090	0.00028	0.00005	0.000025	0.000035	0.000015	$\leq 5\times10^{-6}$	$\leq 5\times10^{-6}$
$g\gamma b\bar{b}$	0.00412	0.00091	0.00030	0.00011	0.00004	$\leq$0.00004	$\leq$0.00004	$\leq$0.00004
$(q/\bar{q})\gamma b\bar{b}$	0.0187	0.0101	0.00662	0.00576	0.00201	0.00115	0.00058	0.00029
Total	0.1213	0.0487	0.0276	0.0254	0.0105	0.0087	0.0062	0.0075

IV. DISCOVERY PROSPECT PROJECTIONS FOR THE 14 TeV LHC

In actual experimental data, the appearance of a peak in the M_X distribution would allow a discovery if it is large enough. The background levels should be determined with some accuracy from data, due to the presence of several sideband control regions. These include events with $M_{\gamma\gamma}$ outside of the window specified in the **S2** cut, events with M_{bb} outside of the window specified in the **S3** cut, and events with M_X outside of the window specified in the **S4** cut. We therefore assume that the determination of backgrounds for the search will be mostly statistical, and set a requirement for a 5-sigma observation of the signal by demanding that $S/\sqrt{B} > 5$, where S and B are the numbers of signal and background events, respectively, that pass the **S4** selection. While this does not account for the "look-elsewhere" effect, it is likely that because of the large luminosities required, by the time a stoponium discovery search becomes relevant, there will be other evidence either from one or both of the channels $\eta_{\tilde{t}} \to \gamma\gamma$ or $\eta_{\tilde{t}} \to ZZ$ or from open stop production, or perhaps from stops obtained from gluino decays. We also require a minimum of $S > 10$ signal events for a discovery, which becomes important when the signal and background cross sections are both low.

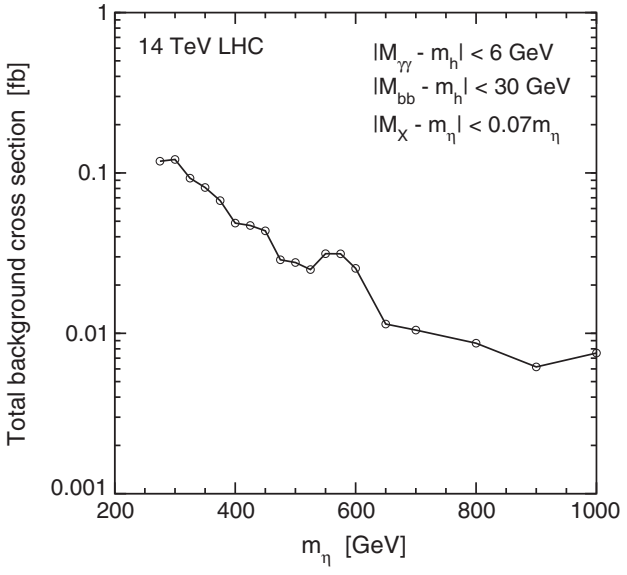

FIG. 5. Total background cross section passing all cuts for event selection **S4**, as a function of m_η, which enters into the M_X cut.

In Fig. 6 we show the cross section $\sigma(pp \to \eta \to hh)$ needed for $S/\sqrt{B} > 5$ and $S > 10$, as a function of m_η, for various integrated luminosities and $\sqrt{s} = 14$ TeV. We see that with an integrated luminosity of 100 fb^{-1} at the 14 TeV LHC, one should be able to discover (or, with the look-elsewhere effect, provide strong evidence for) the resonant process $pp \to \eta \to hh$, provided the cross section exceeds 500 fb to 1.2 pb, depending on the mass. Put another way, a di-Higgs resonance with a cross section for $pp \to \eta \to hh$ of 1.2 pb can be easily discovered with less than 100 fb^{-1} of integrated luminosity, independent of its mass as long as it is larger than about 275 GeV. With 300 fb^{-1}, it may be possible to discover a di-Higgs resonance with a cross section as low as 175–250 fb, if its mass is in the 600–1000 GeV range, although this is limited by statistics. However, for the specific case of stoponium, the expected cross sections fall very steeply with mass. For comparison,

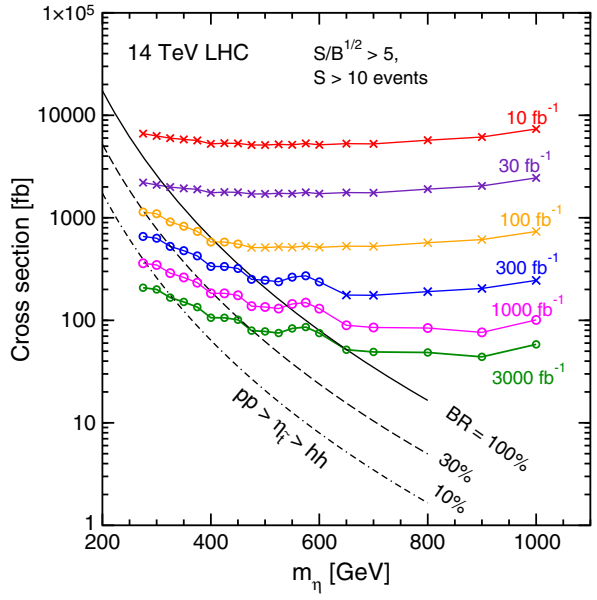

FIG. 6 (color online). The $\sigma(pp \to \eta \to hh)$ cross sections needed for an expected $S/\sqrt{B} > 5$, $S > 10$ event discovery as a function of m_η, for integrated luminosities 10, 30, 100, 300, 1000, and 3000 fb^{-1} in pp collisions at $\sqrt{s} = 14$ TeV. The points marked with a circle are those that have an expected $S/\sqrt{B} = 5$ with $S > 10$ events, while those marked with an X have an expected $S = 10$ events with $S/\sqrt{B} > 5$. Also shown are the predicted cross sections for stoponium production, $\sigma(pp \to \eta_{\tilde{t}} \to hh)$, based on Ref. [9] for NLO $\sigma(pp \to \eta_{\tilde{t}})$ and with assumed BR$(\eta_{\tilde{t}} \to hh) = 100\%$, 30%, 10%.

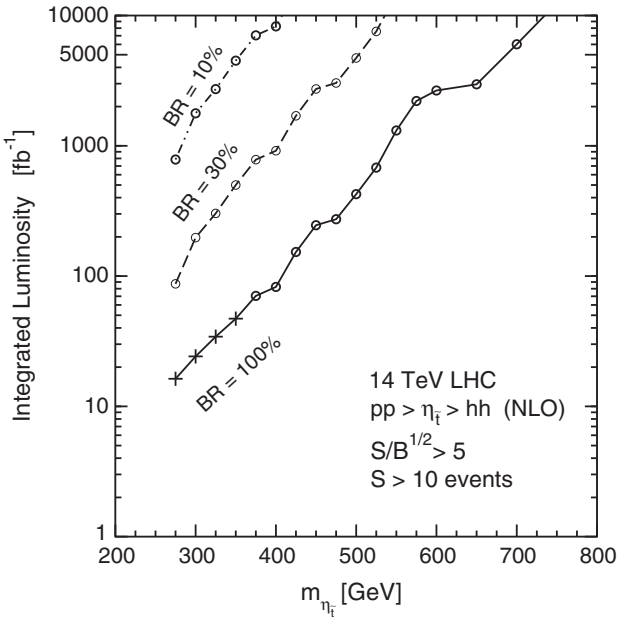

FIG. 7. Total integrated luminosity needed for an expected $S/\sqrt{B} > 5$ and $S > 10$ events, as a function of $m_{\eta_{\tilde{t}}}$, for $pp \to \eta_{\tilde{t}} \to hh$ at $\sqrt{s} = 14$ TeV, taking the NLO cross section for $pp \to \eta_{\tilde{t}}$ from Ref. [9] and assuming 100%, 30%, and 10% branching ratios for $\eta_{\tilde{t}} \to hh$. The points marked with a circle have an expected $S/\sqrt{B} = 5$ and $S > 10$ events, while those marked by a + symbol have an expected $S = 10$ events and $S/\sqrt{B} > 5$.

also shown in Fig. 6 are the predicted cross sections for stoponium production, $\sigma(pp \to \eta_{\tilde{t}} \to hh)$, based on Ref. [9] for $\sigma(pp \to \eta_{\tilde{t}})$ and with assumed BR$(\eta_{\tilde{t}} \to hh) = 100\%$, 30%, and 10%, as indicated. Figure 7 shows the integrated luminosity required for discovery of stoponium as a function of $m_{\eta_{\tilde{t}}}$, for 100%, 30%, and 10% branching ratios of $\eta_{\tilde{t}}$. With as little as 17 fb^{-1} at $\sqrt{s} = 14$ TeV, the LHC could be able to discover the di-Higgs decay of stoponium with $m_{\eta_{\tilde{t}}} = 275$ GeV, if the branching ratio for $\eta_{\eta_{\tilde{t}}} \to hh$ is close to 100%. However, even in this optimistic branching ratio case, the discovery potential with 300 fb^{-1} runs out for stoponium masses heavier than about 500 GeV, corresponding to a 250 GeV top squark. For lower branching ratios, the required integrated luminosity is clearly much higher.

V. OUTLOOK

In this paper we have examined the prospects of detecting stoponium and other di-Higgs resonances in the $b\bar{b}\gamma\gamma$ channel at the LHC with $\sqrt{s} = 14$ TeV. Our results outlined in the previous section can be compared with the heavy Higgs search projections using the same final state made in Ref. [24], which we became aware of while the present paper was in progress. Reference [24] used a somewhat different set of analysis parameters, including a higher b-tagging efficiency of 0.7 compared to our more conservative 0.6, a significantly smaller M_{bb} window, and various other different choices for cuts. Nevertheless, comparing our results to Table III of Ref. [24] for the case of a 300 GeV scalar, we find a quite similar projection for the $S/\sqrt{B}$. Other results in Ref. [24] are based on the particular (α, β) parameter space of two Higgs doublet models, so that direct comparisons are difficult for other mass cases. Our paper is therefore complementary to Ref. [24] in the sense that we presented our projections without tying to a specific model for the production cross section.

In this paper, we did not attempt to make projections for the ability of the LHC to produce 95% confidence level exclusions for stoponium or other di-Higgs resonances, which will be appropriate in the case of an absence of any significant candidate peaks in the $bb\gamma\gamma$ invariant mass distribution. To do this will require more sophisticated analyses techniques, rather than just simple cuts. However, clearly the sensitivity of the LHC to making exclusions should be considerably stronger than the discovery projections made here. Besides the $bb\gamma\gamma$ final state looked at here, other channels with higher rates are worthy of consideration [19–25]. In any case, it should be clear on general grounds that LHC searches for di-Higgs resonances should be a priority in the future, in order to exploit the Higgs discovery as a possible window to new physics.

ACKNOWLEDGMENTS

We thank Jahred Adelman and an anonymous referee for useful comments, and Chul Kim, Ahmad Idilbi, Thomas Mehen, and Yeo Woong Yoon for communications regarding the stoponium production cross-section calculation of Ref. [11]. This work was supported in part by the National Science Foundation Grant No. PHY-1068369 and No. PHY-1417028.

Note added.—After this paper appeared, the ATLAS collaboration released the results [62] for searches for resonant and nonresonant hh production in the $\gamma\gamma bb$ final state, with $\sqrt{s} = 8$ TeV. The 95% exclusion on the cross section at $\sqrt{s} = 8$ TeV varies from 800 to 3500 fb when the resonance mass is less than 500 GeV, and is weaker than expected for some resonance masses below 350 GeV.

[1] G. Aad *et al.* (ATLAS Collaboration), Phys. Lett. B **716**, 1 (2012).
[2] G. Aad *et al.* (ATLAS Collaboration), Report No. ATLAS-CONF-2013-014, 2013.
[3] S. Chatrchyan *et al.* (CMS Collaboration), Phys. Lett. B **716**, 30 (2012).
[4] S. Chatrchyan *et al.* (CMS Collaboration), Report No. CMS-PAS-HIG-12-045, 2012.
[5] M. Drees and M. M. Nojiri, Phys. Rev. Lett. **72**, 2324 (1994).
[6] M. Drees and M. M. Nojiri, Phys. Rev. D **49**, 4595 (1994).
[7] S. P. Martin, Phys. Rev. D **77**, 075002 (2008).
[8] S. P. Martin and J. E. Younkin, Phys. Rev. D **80**, 035026 (2009).
[9] J. E. Younkin and S. P. Martin, Phys. Rev. D **81**, 055006 (2010).
[10] V. Barger, M. Ishida, and W.-Y. Keung, Phys. Rev. Lett. **108**, 081804 (2012).
[11] C. Kim, A. Idilbi, T. Mehen, and Y. W. Yoon, Phys. Rev. D **89**, 075010 (2014).
[12] P. Moxhay and R. W. Robinett, Phys. Rev. D **32**, 300 (1985).
[13] M. J. Herrero, A. Mendez, and T. G. Rizzo, Phys. Lett. B **200**, 205 (1988).
[14] V. D. Barger and W. Y. Keung, Phys. Lett. B **211**, 355 (1988).
[15] H. Inazawa and T. Morii, Phys. Rev. Lett. **70**, 2992 (1993).
[16] D. S. Gorbunov and V. A. Ilyin, J. High Energy Phys. 11 (2000) 011.
[17] D. S. Gorbunov, V. A. Ilyin, and V. I. Telnov, Nucl. Instrum. Methods Phys. Res., Sect. A **472**, 171 (2001).
[18] N. Fabiano, Eur. Phys. J. C **19**, 547 (2001).
[19] T. Plehn, M. Spira, and P. M. Zerwas, Nucl. Phys. **B479**, 46 (1996); **B531**, 655(E) (1998).
[20] U. Baur, T. Plehn, and D. L. Rainwater, Phys. Rev. D **69**, 053004 (2004).
[21] M. J. Dolan, C. Englert, and M. Spannowsky, Phys. Rev. D **87**, 055002 (2013).
[22] J. Liu, X. P. Wang, and S. h. Zhu, arXiv:1310.3634.
[23] J. M. No and M. Ramsey-Musolf, Phys. Rev. D **89**, 095031 (2014).
[24] N. Chen, C. Du, Y. Fang, and L. C. Lu, Phys. Rev. D **89**, 115006 (2014).
[25] S. Chatrchyan *et al.* (CMS Collaboration), Report No. CMS-PAS-HIG-13-025.
[26] G. Aad *et al.* (ATLAS Collaboration), Report No. ATLAS-CONF-2014-005.
[27] E. W. N. Glover and J. J. van der Bij, Nucl. Phys. **B309**, 282 (1988).
[28] S. Dawson, S. Dittmaier, and M. Spira, Phys. Rev. D **58**, 115012 (1998).
[29] U. Baur, T. Plehn, and D. L. Rainwater, Phys. Rev. D **67**, 033003 (2003).
[30] M. J. Dolan, C. Englert, and M. Spannowsky, J. High Energy Phys. 10 (2012) 112.
[31] A. Papaefstathiou, L. L. Yang, and J. Zurita, Phys. Rev. D **87**, 011301 (2013).
[32] J. Baglio, A. Djouadi, R. Gröber, M. M. Mühlleitner, J. Quevillon, and M. Spira, J. High Energy Phys. 04 (2013) 151.
[33] F. Goertz, A. Papaefstathiou, L. L. Yang, and J. Zurita, J. High Energy Phys. 06 (2013) 016.
[34] D. Y. Shao, C. S. Li, H. T. Li, and J. Wang, J. High Energy Phys. 07 (2013) 169.
[35] D. de Florian and J. Mazzitelli, Phys. Lett. B **724**, 306 (2013).
[36] A. J. Barr, M. J. Dolan, C. Englert, and M. Spannowsky, Phys. Lett. B **728**, 308 (2014).
[37] D. de Florian and J. Mazzitelli, Phys. Rev. Lett. **111**, 201801 (2013).
[38] M. J. Dolan, C. Englert, N. Greiner, and M. Spannowsky, Phys. Rev. Lett. **112**, 101802 (2014).
[39] J. R. Espinosa, M. Quiros, and F. Zwirner, Phys. Lett. B **307**, 106 (1993); M. S. Carena, M. Quiros, and C. E. M. Wagner, Phys. Lett. B **380**, 81 (1996); Nucl. Phys. **B524**, 3 (1998); J. R. Espinosa, Nucl. Phys. **B475**, 273 (1996); D. Bodeker, P. John, M. Laine, and M. G. Schmidt, Nucl. Phys. **B497**, 387 (1997); M. S. Carena, M. Quiros, A. Riotto, I. Vilja, and C. E. M. Wagner, Nucl. Phys. **B503**, 387 (1997); J. M. Cline, M. Joyce, and K. Kainulainen, Phys. Lett. B **417**, 79 (1998); **448**, 321(E) (1999); J. High Energy Phys. 07 (2000) 018; J. M. Cline and G. D. Moore, Phys. Rev. Lett. **81**, 3315 (1998); M. S. Carena, M. Quiros, M. Seco, and C. E. M. Wagner, Nucl. Phys. **B650**, 24 (2003); C. Balazs, M. S. Carena, and C. E. M. Wagner, Phys. Rev. D **70**, 015007 (2004); C. Balazs, M. S. Carena, A. Menon, D. E. Morrissey, and C. E. M. Wagner, Phys. Rev. D **71**, 075002 (2005); D. E. Morrissey and M. J. Ramsey-Musolf, New J. Phys. **14**, 125003 (2012).

[40] C. L. Bennett *et al.* (WMAP Collaboration), Astrophys. J. Suppl. Ser. **208**, 20 (2013).
[41] P. A. R. Ade *et al.* (Planck Collaboration), arXiv:1303.5076.
[42] C. Boehm, A. Djouadi, and M. Drees, Phys. Rev. D **62**, 035012 (2000).
[43] J. R. Ellis, K. A. Olive, and Y. Santoso, Astropart. Phys. **18**, 395 (2003).
[44] S. P. Martin, Phys. Rev. D **75**, 115005 (2007); **76**, 095005 (2007).
[45] A. De Simone, G. F. Giudice, and A. Strumia, J. High Energy Phys. 06 (2014) 081.
[46] A. G. Cohen, D. B. Kaplan, and A. E. Nelson, Phys. Lett. B **388**, 588 (1996).
[47] M. Papucci, J. T. Ruderman, and A. Weiler, J. High Energy Phys. 09 (2012) 035.
[48] G. Aad *et al.* (ATLAS Collaboration), Report No. ATLAS-CONF-2013-068.
[49] G. Aad *et al.* (ATLAS Collaboration), Report No. ATLAS-CONF-2013-048.
[50] G. Aad *et al.* (ATLAS Collaboration), J. High Energy Phys. 06 (2014) 124.
[51] S. Chatrchyan *et al.* (CMS Collaboration), Eur. Phys. J. C **73**, 2677 (2013).
[52] S. Chatrchyan *et al.* (CMS Collaboration), Report No. CMS-PAS-SUS-13-009.
[53] K. Krizka, A. Kumar, and D. E. Morrissey, Phys. Rev. D **87**, 095016 (2013).
[54] A. Delgado, G. F. Giudice, G. Isidori, M. Pierini, and A. Strumia, Eur. Phys. J. C **73**, 2370 (2013).
[55] J. A. Evans and Y. Kats, J. High Energy Phys. 04 (2013) 028.
[56] Y. Bai, A. Katz, and B. Tweedie, J. High Energy Phys. 01 (2014) 040.
[57] J. Alwall, M. Herquet, F. Maltoni, O. Mattelaer, and T. Stelzer, J. High Energy Phys. 06 (2011) 128.
[58] T. Sjostrand, S. Mrenna, and P. Z. Skands, J. High Energy Phys. 05 (2006) 026.
[59] S. Chatrchyan *et al.* (CMS Collaboration), Report No. CMS-PAS-SUS-12-018.
[60] G. Aad *et al.* (ATLAS Collaboration), Report No. ATL-PHYS-PUB-2011-007.
[61] J. de Favereau, C. Delaere, P. Demin, A. Giammanco, V. Lemaitre, A. Mertens, and M. Selvaggi, J. High Energy Phys. 02 (2014) 057.
[62] G. Aad *et al.* (ATLAS Collaboration), arXiv:1406.5053.